Dyes and Pigments 98 (2013) 181–189

Contents lists available at SciVerse ScienceDirect

Dyes and Pigments

journal homepage: www.elsevier.com/locate/dyepig

Performance of four artificial chlorin-type sensitizers with different stereostructures in dye-sensitized solar cells

Xiujun Liu [a], Chengjie Li [a], Xiao Peng [a], Yongzhu Zhou [a], Zhe Zeng [a], Yuanchao Li [a], Tianyi Zhang [a], Bao Zhang [a], Yi Dong [b], Dongming Sun [c], Ping Cheng [c], Yaqing Feng [a,*]

[a] School of Chemical Engineering and Technology, Tianjin University, No. 92 Weijin LU, Nankai QU, Tianjin 300072, PR China
[b] Physical and Theoretical Chemistry, University of Saarland, Saarbrücken 66123, Germany
[c] School of Environmental and Chemical Engineering, Shanghai University, Shanghai 200444, PR China

ARTICLE INFO

Article history:
Received 21 November 2012
Received in revised form
14 January 2013
Accepted 15 January 2013
Available online 30 January 2013

Keywords:
Porphyrin
Chlorin
1,3-Dipolar cycloaddition reaction
Dye-sensitized solar cell
Absorption spectra in TiO_2 films
Photovoltaic performance

ABSTRACT

Four artificial chlorin-type sensitizers have been prepared and their photovoltaic performance in dye-sensitized solar cells has been evaluated. It was found that the photovoltaic performance increased with growing absorption intensity of the Q band in a TiO_2 film. This result indicates the contribution of intrinsic enhanced absorption properties of chlorins in the Q band regions on the improvement of the overall photovoltaic performance in DSSCs. On the other hand, their capability of solar energy conversion also exhibits close relationship with the geometry of the four sensitizers, in which the orientation of a sterically demanding 2,6-dichlorophenyl group towards either the 5- or 15-position (the anchor group is at the 20-position) gives higher solar energy-to-electricity conversion efficiency.

1. Introduction

Due to their high solar energy-to-electricity conversion efficiencies, easy fabrication, and low production costs [1], dye sensitized solar cells (DSSCs) have attracted much attention as a new generation of devices to utilize sunlight. Many kinds of sensitizers have been developed, such as triarylamine [2–8], coumarin [9–11], Ru-polypyridyl complexes [12–17], porphyrin [18–27], and other organic sensitizers [28–33]. Among them, porphyrins show special properties with high performance in DSSCs because of their strong absorption and emission in the visible region, tunable redox potentials and structural flexibility (four *meso*-positions and eight β-positions) [34]. So far the best-performing porphyrin dyes have been reported with conversion efficiency around 12% in DSSCs [18]. However, most of the highly efficient porphyrin sensitizers in DSSCs lack the light-harvesting ability in the spectrum ranging from 600 nm to 800 nm. Therefore, it is absolutely necessary to extend the absorption region of the sensitizers to efficiently utilize light energy of more than 600 nm for the future development of DSSCs. Inspired by the role of chlorophylls (17,18-dihydroporphyrin) and bacteriochlorophylls (7,8,17,18-tetrahydroporphyrin) [35–37] in the natural photosynthesis as the main pigments to utilize solar energy over a large window of the solar radiation spectrum, dihydroporphyrins and tetrahydroporphyrins have attracted considerable interest recently [38–43] in terms of powerful solar energy harvesting in the area above 600 nm. In this field, many remarkable contributions have been made by Wang and his co-workers who used chlorophyll derivatives as sensitizers in DSSCs [40–42]. To artificially prepare dihydroporphyrins or tetrahydroporphyrins, numerous methods have been reported, e.g. Diels–Alder reaction [44], reduction by diimide [45], oxidation by OsO_4 [46] and 1,3-dipolar cycloaddition reaction [47–54] on the peripheral double bonds of pyrrolic rings. In connection with our previous study on 1,3-dipolar cycloaddition reaction between A4-porphyrin and nitrile oxides [48], we plan to furnish the chlorin-type framework by this reaction between an A3B-porphyrin and a nitrile oxide, and use the artificial chlorins in DSSCs.

In this paper, we synthesized four chlorin-type sensitizers with strong absorption at long wavelength, and studied their spectral, electro-chemical, and photovoltaic properties, meanwhile we also investigated the influencing factors of the photovoltaic performance of the chlorin-type sensitizers in DSSCs.

* Corresponding author. Tel.: +86 22 27891958; fax: +86 22 27401795.
E-mail address: yqfeng@tju.edu.cn (Y. Feng).

0143-7208/$ – see front matter © 2013 Elsevier Ltd. All rights reserved.
http://dx.doi.org/10.1016/j.dyepig.2013.01.013

2. Experimental section

2.1. Materials and analytical measurements

Dry toluene was prepared by distillation under nitrogen in the presence of sodium and benzophenone ketyl, and dichloromethane (CH_2Cl_2) was distilled before being used for chromatography. Column chromatography (CC): silica gel (300–400 mesh or silica H).

Nuclear magnetic resonance (^{1}H-, ^{1}H-Roesy) spectra: Varian 500 or Bruker AV400; chemical shifts (δ) in ppm, with δ ($CHCl_3$) = 7.26 ppm, δ (DMSO) = 2.50 ppm for ^{1}H NMR. HR-ESI-MS: Bruker microTof-QII, positive ion mode and Bruker Autoflex Tof/Tof III. The X-ray dates: a Rigaku CCD diffractometer using Mo Kα radiation = 0.71073Å, at 113 (2) K. The UV–Vis spectra: Shimadzu UV-1800 in 10 mm quartz cell Spectrometer using EtOH as solvent. The Fluorescence spectra: a Varian Cary Eclipse Spectrometer, emission wavelengths λ in nm and the fluorescence lifetime: HORIBA JY Fluorolog, single electron photoelectric counter (argon saturated EtOH, excitation at 366 nm, detection at the maxima of flourescence). Cyclic voltammetry measurements: CHI 660D (the working electrode and the counter electrode are Pt wires, and a Ag/Ag$^+$ is used as the reference electrode. Fc/Fc$^+$ redox couple is employed for calibration. The electrolyte is n-Bu_4NClO_4 (TBAP, 0.1 M) in dry CH_2Cl_2).

2.2. Synthesis of porphyrins

2.2.1. Synthesis of 5-((4-methoxycarbonyl)phenyl)-10,15,20-triphenylporphyrin (**P$_0$**)

Compound **P$_0$** bearing an ester group was prepared according to the reported methods [55]. The yield of **P$_0$** is 15%, ^{1}H-NMR (400 M Hz, $CDCl_3$): δ −2.76 (s, 2H, pyrrole-NH), 2.71(s, 9H, $-CH_3$), 4.12 (s, 3H, $-COOCH_3$), 7.56 (d, J = 7.5 Hz, 6H, Ph-H), 8.10 (d, J = 7.5 Hz, 6H, Ph-H), 8.31 (d, J = 7.8 Hz, 2H, Ph-H), 8.44 (d, J = 7.8 Hz, 2H, Ph-H), 8.78 (d, J = 4.4 Hz, 2H, pyrrole-H), 8.88(s, 6H, pyrrole-H). HRMS (ESI) ($C_{49}H_{38}N_4O_2$: exact mass = 714.2995): calcd for [M + H]$^+$: 715.3068, found: 715.3069. UV–Vis (CH_2Cl_2) λ_{max} (nm) (ε (10^3 M^{-1} cm^{-1})): 420 (433.3), 517 (16.3), 552 (8.7), 592 (5), 648 (5.3). IR(KBr, cm^{-1}):3021.87, 2920.34, 1726.64, 1609.22, 1560.19, 1507.16, 1436.77, 1275.84, 1107.53, 796.79, 732.84.

2.2.2. General procedure for the 1,3-dipolar cycloadditions

The general procedure of the reaction is described as follows: A toluene (30 mL) solution of porphyrins **P$_0$** (0.1 g, 0.14 mmol) and nitrile oxides (0.7 mmol) was refluxed for 6 h under N_2. Further portion of nitrile oxides (0.7 mmol) was added and the reflux prolonged for an extra period of 6 h. The solvent was then evaporated in vacuo and the residue was purified by column chromatography on silica gel (silica H) to give the cycloadducts

Cyc-1: 10% yield, ^{1}H-NMR (500 MHz, $CDCl_3$): δ −2.01 (s, 1H, pyrrole-NH), −1.94 (s, 1H, pyrrole-NH), 2.53 (s, 3H, $-CH_3$), 2.66 (s, 3H, $-CH_3$), 2.68 (s, 3H, $-CH_3$), 4.09 (s, 3H, $-COOCH_3$), 6.81 (d, J = 7.8 Hz, 1H, Ph-H), 6.86 (d, J = 7.8 Hz, 1H, Cl_2Ph-m-H), 6.91 (d, J = 7.8 Hz, 1H, Ph-H), 7.11 (d, J = 7.8 Hz, 1H, Cl_2Ph-m-H), 7.17 (t, J = 7.8 Hz, 1H, Cl_2Ph-p-H), 7.20 (d, J = 10.1 Hz, 1H, H-7), 7.40 (d, J = 7.8 Hz, 1H, Ph-H), 7.42 (d, J = 7.9 Hz, 1H, Ph-H), 7.53 (s, 2H, Ph-H), 7.57 (d, J = 7.9 Hz, 1H, Ph-H), 7.65 (d, J = 7.7 Hz, 1H, Ph-H), 7.89 (d, J = 10.1 Hz, 1H, H-8), 7.94 (d, J = 7.8 Hz, 1H, Ph-H), 7.97 (s, 1H, Ph-H), 8.08 (d, J = 6.5 Hz, 2H, Ph-H), 8.22 (d, J = 4.5 Hz, 1H, pyrrole-H), 8.35 (d, J = 7.5 Hz, 1H, Ph-H), 8.37–8.46(m, 4H, 1 Ph-H + 3 pyrrole-H), 8.49 (d, J = 7.7 Hz, 1H, Ph-H), 8.51 (d, J = 4.5 Hz, 1H, pyrrole-H), 8.55 (d, J = 4.5 Hz, 1H, pyrrole-H), 8.71 (d, J = 4.5 Hz, 1H, pyrrole-H). Assignments aided by ^{1}H ROESY spectra. HRMS (ESI) ($C_{56}H_{41}Cl_2N_5O_3$: exact mass = 901.2586): calcd for [M + H]$^+$: 902.2659, found: 902.2658. UV–Vis (CH_2Cl_2) λ_{max} (nm) (ε (10^3 M^{-1} cm^{-1})): 419 (192), 522 (14.7), 551 (16.7), 592 (8.3), 646 (21). IR(KBr, cm^{-1}): 3023.69, 2951.19, 2921.48, 1723.45, 1609.50, 1568.29, 1517.07, 1431.52, 1277.77, 1108.20, 790.35, 718.45.

Cyc-2: 9.2% yield, ^{1}H-NMR (400 MHz, CDCl3): δ −1.98 (s, 1H, pyrrole-NH), −1.92 (s, 1H, pyrrole-NH), 2.53 (s, 3H, $-CH_3$), 2.66 (s, 3H, $-CH_3$), 2.67 (s, 3H, $-CH_3$), 4.09 (s, 3H, $-COOCH_3$), 6.80 (d, J = 7.7 Hz, 1H, Ph-H), 6.86 (d, J = 7.8 Hz, 1H, Cl_2Ph-m-H), 6.91 (d, J = 7.7 Hz, 1H, Ph-H), 7.11 (d, J = 7.8 Hz, 1H, Cl_2Ph-m-H), 7.16 (t, J = 7.8 Hz, 1H, Cl_2Ph-p-H), 7.19 (d, J = 10.1 Hz, 1H, H-8), 7.40 (d, J = 7.9 Hz, 1H, Ph-H), 7.42 (d, J = 7.9 Hz, 1H, Ph-H), 7.48 (d, J = 7.9 Hz, 1H, Ph-H), 7.54–7.57 (m, 2H, Ph-H), 7.65 (d, J = 7.9 Hz, 1H, Ph-H), 7.85 (d, J = 7.9 Hz, 1H, Ph-H), 7.88 (d, J = 10.1 Hz, 1H, H-7), 7.93 (d, J = 7.9 Hz, 1H, Ph-H), 8.16–8.20 (m, 3H, 2 Ph-H + 1 pyrrole-H), 8.27 (d, J = 8.0 Hz, 1H, Ph-H), 8.40–8.44(m, 4H, 2 Ph-H + 2 pyrrole-H), 8.48 (d, J = 7.9 Hz, 1H, Ph-H), 8.53 (d, J = 4.5 Hz, 1H, pyrrole-H), 8.60 (d, J = 4.5 Hz, 2H, pyrrole-H). Assignments aided by ^{1}H ROESY spectra. HRMS (ESI) ($C_{56}H_{41}Cl_2N_5O_3$: exact mass = 901.2586): calcd for [M + H]$^+$: 902.2659, found: 902.2667. UV–Vis (CH_2Cl_2) λ_{max} (nm) (ε (10^3 M^{-1} cm^{-1})): 418 (191.3), 522 (15.7), 549 (17.3), 594 (8.7), 646 (21.3). IR(KBr, cm^{-1}): 3349.19, 3023.22, 2949.06, 2918.64, 1721.43, 1606.17, 1567.84, 1515.69, 1432.53, 1279.26, 1108.63, 792.10, 716.37.

Cyc-3: 8.9% yield, ^{1}H-NMR (400 MHz, $CDCl_3$): δ −1.86 (s, 1H, pyrrole-NH), −1.81 (s, 1H, pyrrole-NH), 2.66–2.68 (m, 9H, $-CH_3$), 4.08 (s, 3H, $-COOCH_3$), 6.89 (d, J = 8.0 Hz, 1H, Cl_2Ph-m-H), 7.07 (d, J = 8.0 Hz, 1H, Cl_2Ph-m-H), 7.11 (d, J = 10.2 Hz, 1H, H-18), 7.12 (d, J = 7.5 Hz, 1H, Ph-H), 7.20 (t, J = 8.0 Hz, 1H, Cl_2Ph-p-H), 7.42 (d, J = 7.6 Hz, 1H, Ph-H), 7.47 (d, J = 7.9 Hz, 1H, Ph-H), 7.51–7.57 (m, 4H, Ph-H), 7.65 (d, J = 7.8 Hz, 1H, Ph-H), 7.71 (d, J = 7.5 Hz, 1H, Ph-H), 7.85 (s, 1H, Ph-H), 7.89 (d, J = 10.2 Hz, 1H, H-17), 7.97 (s 1H, Ph-H), 8.07 (d, J = 4.4 Hz, 2H, 1 Ph-H + 1 pyrrole-H), 8.15 (d, J = 7.6 Hz, 1H, Ph-H), 8.18 (d, J = 7.9 Hz, 1H, Ph-H), 8.27 (d, J = 7.6 Hz, 1H, Ph-H), 8.40 (d, J = 4.5 Hz, 1H, pyrrole-H), 8.48 (d, J = 7.8 Hz, 1H, Ph-H), 8.51 (s, 2H, pyrrole-H), 8.59 (d, J = 4.4 Hz, 1H, pyrrole-H), 8.69 (d, J = 4.5 Hz, 1H, pyrrole-H). Assignments aided by ^{1}H ROESY spectra. HRMS (ESI) ($C_{56}H_{41}Cl_2N_5O_3$: exact mass = 901.2586): calcd for [M + H]$^+$: 902.2659, found: 902.2638. UV–Vis (CH_2Cl_2) λ_{max} (nm) (ε (10^3 M^{-1} cm^{-1})): 416 (217.3), 521 (16.3), 550 (20), 593 (9.7), 645(25.3). IR(KBr, cm^{-1}): 3349.20, 3020.67, 2947.46, 2917.91, 1722.33, 1604.38, 1567.30, 1514.18, 1433.11, 1276.12, 1106.74, 792.50, 718.04.

Cyc-4: 9.5% yield, ^{1}H-NMR (400 MHz, CDCl3): δ −1.90 (s, 1H, pyrrole-NH), −1.81 (s, 1H, pyrrole-NH), 2.53 (s, 3H, $-CH_3$), 2.67 (s, 6H, $-CH_3$), 4.08 (s, 3H, $-COOCH_3$), 6.80 (d, J = 7.2 Hz, 1H, Ph-H), 6.85 (d, J = 8.0 Hz, 1H, Cl_2Ph-m-H), 6.89 (d, J = 7.2 Hz, 1H, Ph-H), 7.11 (d, J = 8.0 Hz, 1H, Cl_2Ph-m-H), 7.15 (t, J = 8.0 Hz, 1H, Cl_2Ph-p-H), 7.18 (d, J = 10.2 Hz, 1H, H-17), 7.40 (d, J = 7.5 Hz, 1H, Ph-H), 7.47 (d, J = 7.7 Hz, 1H, Ph-H), 7.49–7.57 (m, 3H, Ph-H), 7.79 (d, J = 8.3 Hz, 1H, Ph-H), 7.82 (d, J = 10.2 Hz, 1H, H-18), 7.86 (d, J = 7.3 Hz, 1H, Ph-H), 7.90–8.00 (m, 2H, Ph-H), 8.06 (s, 1H, Ph-H), 8.18 (d, J = 4.6 Hz, 2H, 1 Ph-H + 1 pyrrole-H), 8.30 (d, J = 4.5 Hz, 1H, pyrrole-H), 8.31 (d, J = 8.3 Hz, 1H, Ph-H), 8.48–8.55 (m, 3H, 1 Ph-H + 2 pyrrole-H), 8.59 (d, J = 4.6 Hz, 1H, pyrrole-H), 8.65–8.75 (m, 2H, 1 Ph-H + 1 pyrrole-H). Assignments aided by ^{1}H ROESY spectra. HRMS (ESI) ($C_{56}H_{41}Cl_2N_5O_3$: exact mass = 901.2586): calcd for [M + H]$^+$: 902.2659, found: 902.2658. UV–Vis (CH_2Cl_2) λ_{max} (nm) (ε (10^3 M^{-1} cm^{-1})): 417 (170.3), 522 (13), 550 (16), 594 (8.3), 645(20.3). IR(KBr, cm^{-1}): 3350.82, 3021.35, 2922.32, 2855.82, 1723.69, 1605.01, 1568.30, 1515.15, 1433.99, 1277.28, 1108.59, 791.63, 725.82.

Cyc-5: 9.8% yield, ^{1}H-NMR (400 MHz, $CDCl_3$): δ −2.01 (s, 1H, pyrrole-NH), −1.91 (s, 1H, pyrrole-NH), 2.51 (s, 6H, $-CH_3$), 2.64 (s, 3H, $-CH_3$), 4.07 (s, 3H, $-COOCH_3$), 6.83 (d, J = 7.6 Hz, 2H, Ph-H), 6.86–6.93 (m, 4H, 2 Cl_2Ph-m-H + 2 Ph-H), 7.01 (dd, J = 2.1 Hz, 10.0 Hz, 2H, H-8, H-17), 7.11 (d, J = 7.8 Hz, 2H, Cl_2Ph-m-H), 7.18 (t, J = 7.8 Hz, 2H, Cl_2Ph-p-H), 7.36 (d, J = 7.6 Hz, 2H, Ph-H), 7.44 (d, J = 7.8 Hz, 1H, Ph-H), 7.60 (d, J = 7.5 Hz, 1H, Ph-H), 7.68

(d, J = 10.0 Hz, 1H, H-7), 7.70 (d, J = 7.8 Hz, 1H, Ph-H), 7.74 (d, J = 10.0 Hz, 1H, H-18), 7.80–7.88 (m, 4H, 2 Ph-H + 2 pyrrole-H), 7.93 (d, J = 7.8 Hz, 1H, Ph-H), 8.11 (d, J = 4.4 Hz, 1H, pyrrole-H), 8.23 (d, J = 4.4 Hz, 1H, pyrrole-H), 8.28 (d, J = 7.5 Hz, 1H, Ph-H), 8.34 (d, J = 7.8 Hz, 1H, Ph-H), 8.48 (q, J = 8.4 Hz, 2H, Ph-H). Assignments aided by ^{1}H ROESY spectra. HRMS (ESI) ($C_{63}H_{44}Cl_4N_6O_4$: exact mass = 1088.2178): calcd for $[M + H]^+$: 1089.2251, found: 1089.2247. Crystallographic data for **Cyc-5**: $C_{63}H_{44}Cl_4N_6O_4$, Mw = 1090.87, monoclinic, space group Cc, a = 12.465(10), b = 32.62(3), c = 15.008(15) Å, α = 90, β = 99.42(5), γ = 90 , V = 6020(9) Å^3, Dc = 1.212 g/cm^3, Z = 4, R_1 = 0.1272(4641), wR_2 = 0.3649(10162). UV–Vis (CH_2Cl_2) λ_{max} (nm) (ε (10^3 M^{-1} cm^{-1})): 389 (192.7), 538 (40.3), 644 (5.7), 704(68.7). IR(KBr, cm^{-1}):3428.07, 3020.42, 2950.71, 2917.84, 2861.26, 1724.88, 1605.32, 1571.26, 1505.81, 1428.22, 1272.59, 1071.03, 795.37, 729.33.

2.2.3. Synthesis of chlorin-type dye sensitizers

A mixed solution of free-base monoadducts (0.01 mmol) in $CHCl_3$ (18 mL) and $Zn(OAc)_2 \cdot 2H_2O$ (4.39 mg, 0.02 mmol) in MeOH were refluxed for 30 min, and the reaction mixture was filtered through a short silica pad to give the zinc monoadducts. Then, the zinc monoadducts was dissolved in THF/EtOH/H_2O (8 mL/8 mL/2 mL), and KOH (30 equiv) was added. The reaction was refluxed for 30 min, subsequently, the reaction mixture was acidified by diluted HCl (5%) to adjust pH <7. Next, the mixture was extracted by CH_2Cl_2 to collect the organic layer which was washed with water, dried and concentrated. Chromatography (CH_2Cl_2: MeOH = 50:1) afforded chlorin-type sensitizers.

Dye-1: 6.8 mg, 72%, ^{1}H-NMR (500 MHz, DMSO): δ 2.45 (s, 3H, –CH_3), 2.60 (s, 3H, –CH_3), 2.62 (s, 3H, –CH_3), 6.69 (d, J = 7.6 Hz, 1H, Ph-H), 6.84 (d, J = 7.6 Hz, 1H, Ph-H), 7.17 (d, J = 10.6 Hz, 1H, H-7), 7.17 (d, J = 7.5 Hz, 1H, Ph-H), 7.34 (t, J = 8.0 Hz, 2H, Cl_2Ph-m-H), 7.41 (t, J = 8.0 Hz, 1H, Cl_2Ph-p-H), 7.43 (d, J = 7.7 Hz, 1H, Ph-H), 7.50–7.62 (m, 4H, Ph-H), 7.76 (d, J = 10.6 Hz, 1H, H-8), 7.83 (d, J = 7.0 Hz, 1H, Ph-H), 7.94 (d, J = 4.5 Hz, 1H, pyrrole-H), 7.99 (d, J = 6.5 Hz, 3H, Ph-H), 8.11 (d, J = 4.5 Hz, 1H, pyrrole-H), 8.19 (d, J = 7.7 Hz, 1H, Ph-H), 8.23 (d, J = 7.7 Hz, 1H, Ph-H), 8.26 (d, J = 4.6 Hz, 1H, pyrrole-H), 8.27–8.35 (m, 4H, 2 Ph-H + 2 pyrrole-H), 8.45 (d, J = 4.6 Hz, 1H, pyrrole-H), 13.16 (s, br. H, –COOH). MALDI Tof: m/z calcd for $C_{55}H_{37}Cl_2N_5O_3Zn$ 949.16; found 949.30 $[M]^+$. UV–Vis (CH_2Cl_2) λ_{max} (nm) (ε (10^3 M^{-1} cm^{-1})): 420(240.7), 586(9.7), 614(27.7). IR(KBr, cm^{-1}): 3435.66, 3020.08, 2919.82, 1689.01, 1607.60, 1574.84, 1507.60, 1428.22, 1341.06, 1108.87, 791.47, 717.66.

Dye-2: 6.5 mg, 68%, ^{1}H-NMR (500 MHz, DMSO): δ 2.45 (s, 3H, –CH_3), 2.60 (s, 3H, –CH_3), 2.60 (s, 3H, –CH_3), 6.70 (d, J = 7.8 Hz, 1H, Ph-H), 6.84 (d, J = 7.8 Hz, 1H, Ph-H), 7.17 (d, J = 10.7 Hz, 1H, H-8), 7.18 (d, J = 8.0 Hz, 1H, Ph-H), 7.34 (t, J = 7.9 Hz, 2H, Cl_2Ph-m-H), 7.42 (t, J = 7.9 Hz, 1H, Cl_2Ph-p-H), 7.43 (d, J = 7.8 Hz, 1H, Ph-H), 7.48 (d, J = 7.3 Hz, 1H, Ph-H), 7.54–7.62 (m, 3H, Ph-H), 7.76 (d, J = 10.7 Hz, 2H, H-7 + 1 Ph-H), 7.92 (d, J = 4.5 Hz, 1H, pyrrole-H), 7.99 (d, J = 7.9 Hz, 1H, Ph-H), 8.06 (d, J = 7.2 Hz, 2H, Ph-H), 8.12 (d, J = 4.5 Hz, 1H, pyrrole-H), 8.19 (d, J = 7.9 Hz, 1H, Ph-H), 8.22 (d, J = 7.7 Hz, 1H, Ph-H), 8.27 (d, J = 4.5 Hz, 2H, 1 pyrrole-H + 1 Ph-H), 8.31 (d, J = 4.5 Hz, 2H, 1 pyrrole-H + 1 Ph-H), 8.36 (d, J = 4.5 Hz, 1H, pyrrole-H), 8.41 (d, J = 4.5 Hz, 1H, pyrrole-H), 13.17 (s, br. H, –COOH). MALDI Tof: m/z calcd for $C_{55}H_{37}Cl_2N_5O_3Zn$ 949.16; found 949.20 $[M]^+$. UV–Vis (CH_2Cl_2) λ_{max} (nm) (ε (10^3 M^{-1} cm^{-1})): 420(241.3), 586(12.3), 613(28.7). IR(KBr, cm^{-1}):3433.08, 3020.69, 2920.01, 1731.28, 1607.65, 1574,69, 1507.97, 1429.48, 1341.51, 1109.03, 793.04, 719.40.

Dye-3: 6.6 mg, 70%, ^{1}H-NMR (500 MHz, DMSO): δ 2.59 (s, 6H, –CH_3), 2.61 (s, 3H, –CH_3), 7.03 (d, J = 7.8 Hz, 1H, Ph-H), 7.11 (d, J = 10.6 Hz, 1H, H-18), 7.16 (d, J = 8.2 Hz, 1H, Cl_2Ph-m-H), 7.19 (d, J = 8.2 Hz, 1H, Cl_2Ph-m-H), 7.42 (t, J = 8.2 Hz, 1H, Cl_2Ph-p-H), 7.43 (d, J = 7.5 Hz, 1H, Ph-H), 7.47 (d, J = 7.8 Hz, 1H, Ph-H), 7.51 (d, J = 7.6 Hz, 2H, Ph-H), 7.53–7.61 (m, 4H, Ph-H), 7.75 (d, J = 7.6 Hz, 1H, Ph-H), 7.77 (d, J = 10.6 Hz, 1H, H-17), 7.82 (d, J = 7.2 Hz, 1H, Ph-H), 7.86 (d, J = 4.5 Hz, 1H, pyrrole-H), 7.99 (d, J = 7.2 Hz, 1H, Ph-H), 8.05 (d, J = 7.8 Hz, 1H, Ph-H), 8.09 (d, J = 4.5 Hz, 1H, pyrrole-H), 8.11 (d, J = 8.2 Hz, 1H, Ph-H), 8.18 (d, J = 7.8 Hz, 1H, Ph-H), 8.24 (d, J = 7.8 Hz, 1H, Ph-H), 8.29 (q, J = 4.5 Hz, 2H, pyrrole-H), 8.34 (d, J = 4.5 Hz, 1H, pyrrole-H), 8.43 (d, J = 4.5 Hz, 1H, pyrrole-H). MALDI Tof: m/z calcd for $C_{55}H_{37}Cl_2N_5O_3Zn$ 949.16; found 949.32 $[M]^+$. UV–Vis (CH_2Cl_2) λ_{max} (nm) (ε (10^3 M^{-1} cm^{-1})): 418(243.3), 585(11.7), 612(28). IR(KBr, cm^{-1}):3417.00, 3021.48, 2919.45, 1733.55, 1606.64, 1572.43, 1506.29, 1429.79, 1341.49, 1079.50, 795.42, 728.86.

Dye-4: 6.3 mg, 66%, ^{1}H-NMR (500 MHz, DMSO): δ 2.45 (s, 3H, –CH_3), 2.60 (s, 3H, –CH_3), 2.61 (s, 3H, –CH_3), 6.70 (d, J = 7.4 Hz, 1H, Ph-H), 6.80 (d, J = 7.4 Hz, 1H, Ph-H), 7.14 (d, J = 10.7 Hz, 1H, H-17), 7.16 (d, J = 7.9 Hz, 1H, Ph-H), 7.31–7.37 (m, 2H, Cl_2Ph-m-H), 7.41 (t, J = 8.1 Hz, 1H, Cl_2Ph-p-H), 7.48 (d, J = 7.7 Hz, 1H, Ph-H), 7.52 (d, J = 7.5 Hz, 1H, Ph-H), 7.55 (d, J = 7.6 Hz, 2H, Ph-H), 7.75 (d, J = 7.5 Hz, 1H, Ph-H), 7.78 (d, J = 10.7 Hz, 1H, H-18), 7.82 (d, J = 6.7 Hz, 2H, Ph-H), 7.90 (d, J = 4.5 Hz, 1H, pyrrole-H), 7.96–8.02 (m, 2H, Ph-H), 8.03–8.08 (m, 2H, 1 pyrrole-H + 1 Ph-H), 8.20 (d, J = 8.0 Hz, 1H, Ph-H), 8.30 (q, J = 4.5 Hz, 2H, pyrrole-H), 8.34 (d, J = 4.5 Hz, 1H, pyrrole-H), 8.35–8.41 (m, 2H, Ph-H), 8.44 (d, J = 4.5 Hz, 1H, pyrrole-H), 13.15 (s, br. H, –COOH). MALDI Tof: m/z calcd for $C_{55}H_{37}Cl_2N_5O_3Zn$ 949.16; found 949.42 $[M]^+$. UV–Vis (CH_2Cl_2) λ_{max} (nm) (ε (10^3 M^{-1} cm^{-1})): 418(239), 585(13), 612(29.7). IR(KBr, cm^{-1}): 3428.07, 3020.42, 2917.84, 1724.88, 1605.32, 1571.26, 1505.81, 1428.82, 1340.23, 1071.03, 795.37, 729.33.

2.3. Absorption spectra on TiO_2 films

Absorption spectra of the sensitizers deposited on TiO_2 films were measured with a Shimadzu UV-1800 spectrometer. The TiO_2 films with a typical thickness of 5 μm were dipped into 0.3 mM ethanol solution of chlorin dyes for 15 min and then the dye-adsorbed films are rinsed with ethanol three times and dried in air before measurement of the absorption spectra.

2.4. Measurement of surface coverage (Γ)

TiO_2 films 0.16 cm^2 in size, ~16 μm in thickness were dipped into an ethanolic solution containing each dye sensitizer for 2 h and then washed with ethanol to remove free dye sensitizers on the surface. The adsorbed dye sensitizers were estimated when dissolved in 3 mL of 0.1 M EtONa solution. The absorption spectra of the EtONa solution of each sensitizer were measured to obtain the surface coverage (Γ) according to the standard method [56].

2.5. Fabrication of DSSCs and photovoltaic measurements

The optically transparent electrode (OTE) with 0.16 cm^2 working area contains 20 nm TiO_2 nanoparticles with thickness of 12 μm and 400 nm TiO_2 nanoparticles (diffusive layer) with thickness of 4 μm was prepared by screen print for light-harvesting. The electrolyte consisted of 0.06 M LiI, 0.03 M I_2, 0.6 M 1,2-dimethyl-3-propylimidazolium iodide (DMPII), and 0.5 M 4-tert-butylpyridine (TBP) in a mixture of acetonitrile and valeronitrile (volume ratio, 85: 15) [57]. The porphyrin dyes sensitized TiO_2 electrodes were measured under simulated AM 1.5 irradiation (100 mW/cm^2) and the photocurrent–voltage (J–V) characteristics were recorded on Keithley 2400 Source meter (solar AAA simulator, oriel China, calibrated with a standard crystalline silicon solar). The power conversion efficiency (η) of the DSSCs was calculated from short-circuit photocurrent (J_{sc}), the open-circuit photovoltage (V_{oc}), the fill factor (FF) and the intensity of the incident light (P_{in}) according to the following equation:

$$\eta = \frac{J_{sc}(\mathrm{mA/cm^2}) \times V_{oc}(\mathrm{V}) \times \mathrm{FF}}{P_{in}(\mathrm{mW/cm^2})}$$

The action spectra of monochromatic incident photon-to-current conversion efficiency (IPCE) for the solar cells were performed by using a commercial setup (QTest Station 2000 IPCE Measurement System, CROWNTECH, USA).

2.6. Theoretical calculations

Full ground geometry optimization of dyes was carried out by using DFT calculation with B3LYP exchange-correlations functional and the 6-31G(d, p) basis set and with CPCM solvent model (EtOH) [43,58–62]. The TD-DFT calculations with the BP 86 exchange-correlations functional and the 6-31G(d, p) basis set were based on the optimized structure with solvation effect described by CPCM (EtOH) for the set of sensitizers [63–68].

3. Results and discussions

3.1. Synthesis and characterization

The synthetic route to artificial chlorin-type sensitizers is depicted in Scheme 1. Here, **P_0** [55] was treated with nitrile oxide [47,48] so that the reaction substances underwent the typical 1,3-dipolar cycloaddition reaction affording both the monoadducts and the bisadducts. The chlorin-type sensitizers were then obtained after the metallization of the monoadducts and following hydrolysis of the COOMe group. In detail, the solution of **P_0** and an excess of nitrile oxides in toluene was heated to reflux under N_2

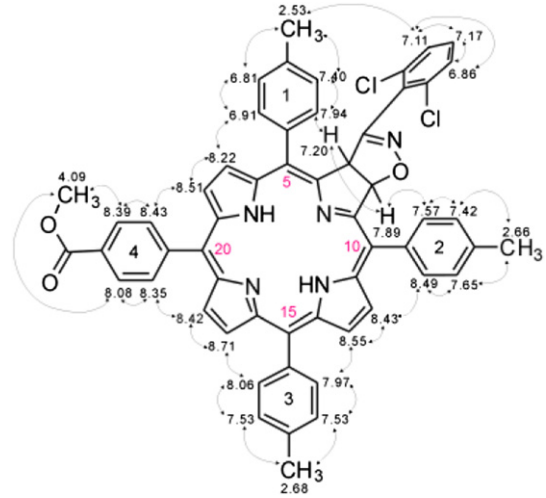

Fig. 1. ^{1}H-chemical shift data with 2D ROESY correlations for compound **Cyc-1**.

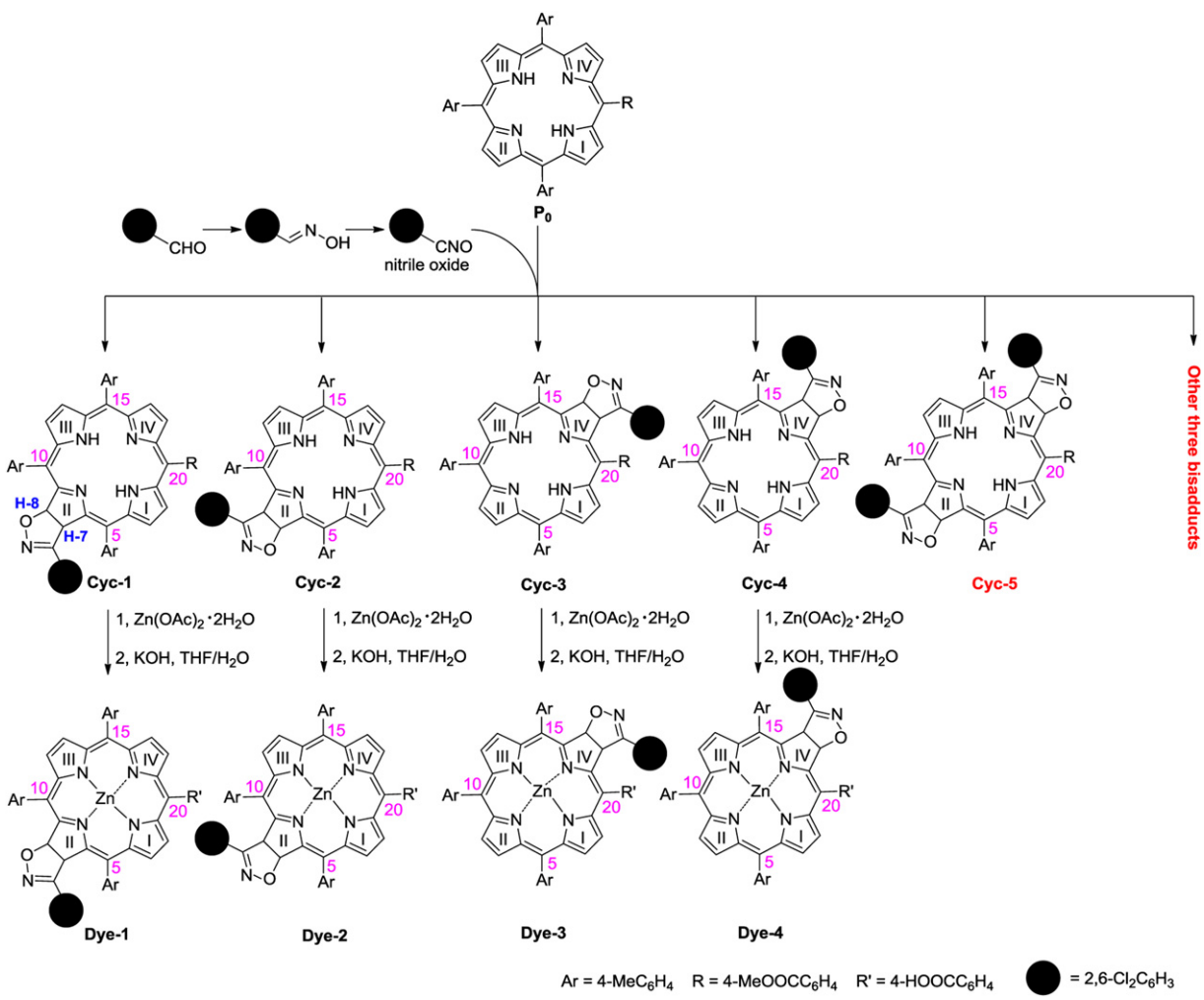

Scheme 1. The synthetic route to the chlorin-type sensitizers.

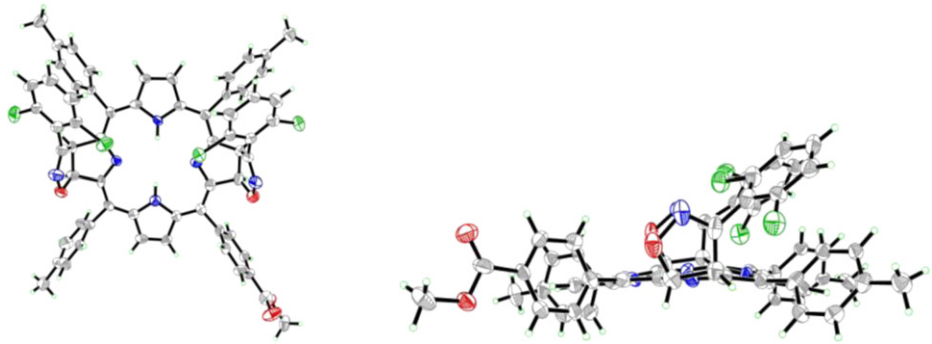

Fig. 2. The crystal structure of the bisadduct **Cyc-5** (left: front view, right: side view).

until TLC revealed no further progress of the reaction. Subsequently, metallization of the free base monoadducts with $Zn(OAc)_2 \cdot 2H_2O$, followed by alkaline hydrolysis of the COOMe group, gave the chlorin-type sensitizers. As $\mathbf{P_0}$ was a A3B-type porphyrin, there should be a certain selectivity to form monoadducts in the cycloaddition reaction. However, four monoadducts with similar yields were isolated and demonstrated the equal reactivity of the peripheral double bonds in pyrrolic rings of this kind of A3B-porphyrin. In addition, *o*-dichlorobenzene was also employed as an alternative to toluene as the solvent in the 1,3-dipolar cycloaddition reaction, but the yield decreased sharply due to the elevated reaction temperature.

The respective structures of the four isomeric monoadducts were deduced from one- and two-dimensional ^{1}H-NMR spectroscopy. In the ^{1}H-NMR spectra of monoadducts (Figure S8–S11 in Supplementary Materials), the split of the signals corresponding to β-protons and phenyl protons were detected at low field. These changes demonstrate the lower symmetry of the porphyrin framework after the cycloaddition reaction. Meanwhile, two sets of doublets ($J = 9.8–10.7$ Hz) were observed at the similar chemical shift values, suggesting their assignment as that of saturated pyrrolic protons (H-7 and H-8 or H-17 and H-18). The identification of the cycloaddition site was achieved by tracing the H–H correlations of the monoadducts. Here, we took the analysis of **Cyc-1** as an example (Fig. 1 and Figure S1 in Supplementary Materials). First, we marked the *meso*-benzene rings with CH_3 as **1**, **2**, **3** according to the chemical shift value of the CH_3 group at 2.53 ppm, 2.66 ppm, 2.68 ppm, respectively, and the *meso*-benzene ring with $COOCH_3$ as **4**. On the basis of the coupling between the protons in the CH_3 or $COOCH_3$ group and the protons in *meso*-benzene rings themselves, eight aromatic protons belonging to different benzene rings were found, e.g. the coupling partner of CH_3 (2.53 ppm) at 6.81 ppm and 7.40 ppm could be assigned to the aromatic protons in benzene ring **1**. Then, because of the correlation between the known eight aromatic protons and the unknown eight aromatic protons in benzene rings, the signals of the protons in four *meso*-benzene rings were obtained. The protons of the saturated pyrrolic ring at 7.20 ppm and 7.89 ppm were coupling with the aromatic protons at 7.94 ppm (of the benzene ring **1**) and 7.57 ppm (of the benzene ring **2**). This result indicates the occurrence of the cycloaddition reaction on the pyrrolic ring between two 4-methylphenyl groups. In addition, another signal of aromatic proton in benzene ring **1** (6.91 ppm) correlated to the proton with the signal at 8.22 ppm ($J = 4.5$ Hz) which should be assigned to the unsaturated pyrrolic proton. Following another coupling of the signal with that of the unsaturated pyrrolic ring proton at 8.22 ppm, the other pyrrolic proton signal at 8.51 ppm ($J = 4.5$ Hz) was picked up. As the signals at 8.43 ppm which were assigned to the aromatic proton in 4-CH_3COOPh group correlated to pyrrolic proton signal at 8.51 ppm, the four *meso*-substituted aromatic rings and cycloaddition reaction site were identified besides the spatial orientation of the 2,6-dichlorophenyl group. On the basis of the coupling between the signal at 2.53 ppm from benzene ring **1** and signal at 7.11 ppm (of the aromatic proton in 2,6-dichlorophenyl group), the orientation of the 2,6-dichlorophenyl group was confirmed to point towards benzene ring **1** which was next to the 4-carboxymethylphenyl group. So the exact structure of this monoadduct was established. By the same way, the structures of the other three monoadducts were established.

In addition, four bisadducts were also separated in the cycloaddition. One of the bisadducts **Cyc-5** has been characterized by X-ray analysis (Fig. 2). In its structure, the two 2,6-dichlorophenyl groups were added to the opposite pyrrolic ring in the same orientation. The structures of the other three bisadducts have not yet been fully elucidated.

3.2. Optical and electrochemical properties

The molecular structures of the four chlorin sensitizers **Dye-1**, **Dye-2**, **Dye-3** and **Dye-4** were exhibited in Fig. 3. And their UV–Vis

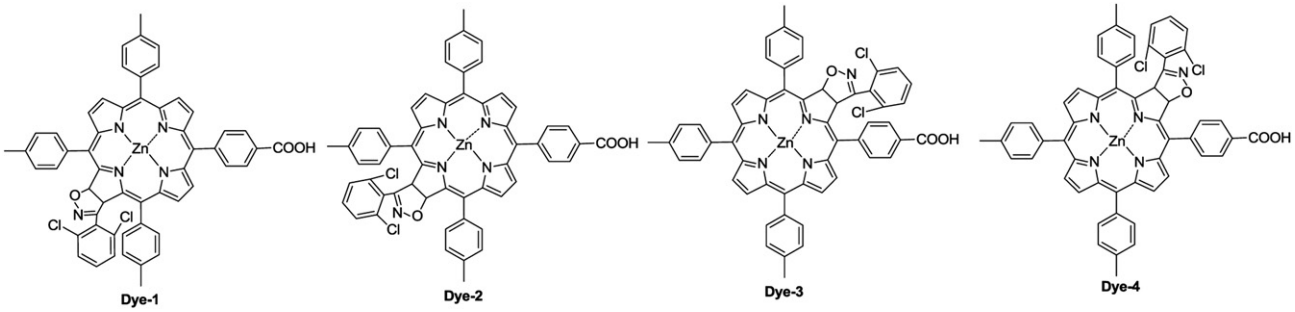

Fig. 3. The molecular structures of four chlorin sensitizers **Dye-1**, **Dye-2**, **Dye-3** and **Dye-4**.

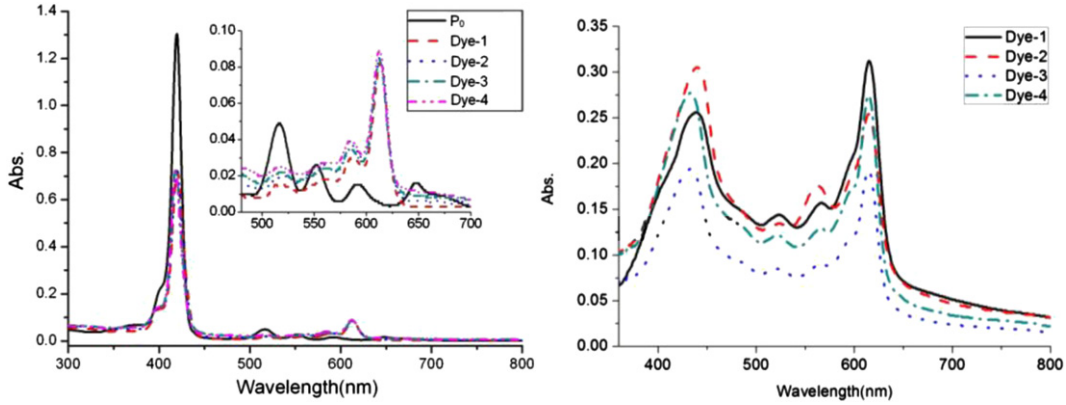

Fig. 4. The UV–Vis spectra of $\mathbf{P_0}$, **Dye-1**, **Dye-2**, **Dye-3** and **Dye-4** in EtOH (3×10^{-6} mol/L) (left) and the UV–Vis spectra of **Dye-1**, **Dye-2**, **Dye-3** and **Dye-4** on TiO_2 films (5 μm) (right).

spectra in EtOH are shown in Fig. 4 (left). The absorption maxima and extinction coefficients for the Soret- and Q-bands of all products are listed in Table 1. Compared with the spectrum of $\mathbf{P_0}$, the spectra of four chlorin-type sensitizers show a distinct red-shift and higher molar extinction coefficients in the 600 nm–620 nm spectral ranges due to the partial saturated pyrrolic ring resulting from the cycloaddition reaction [47,69], which is accompanied by lower molar extinction coefficients of their Soret bands. In addition, the Soret bands of **Dye-3** and **Dye-4** show a ~2 nm blue shift compared with that of the **Dye-1** and **Dye-2**. This phenomena indicates greater distortion of the porphyrin framework when the dichlorophenyl is introduced to the pyrrolic ring IV (Scheme 1).

The light-harvesting capability of the dyes is a significant parameter which determines the amount of solar energy that can be captured by DSSCs and consequently affects the photocurrent generated. Fig. 4 (right) exhibits the UV–Vis spectra of the four chlorin-type sensitizers anchored on the TiO_2 films (5 μm). Compared to the sensitizers in solution, the anchorage onto TiO_2 films shifts the absorption peaks to a longer wavelength region together with a substantially broadened bandwidth. These changes may attribute to the J-type aggregation of the dyes on the TiO_2 surface [70]. Furthermore, the absorption intensity of the Q bands of the sensitizers behaves similar to that of Soret bands and are in the order **Dye-1** > **Dye-4** > **Dye-2** > **Dye-3**. Here, we should emphasize that the Q band absorption intensity of **Dye-1** is even stronger than that of the Soret band. The enhancement of the Q bands absorption after being deposited on TiO_2 films proposes the dominant role of Q bands absorption in light-harvesting and light-converting for this kind of sensitizers.

The steady-state fluorescence spectra of the four chlorin-type sensitizers, exhibited in Fig. 5, was obtained in EtOH with excitation wavelength at 420 nm. The spectra show characteristic vibronic bands for **Dye-1**, **Dye-2**, **Dye-3** and **Dye-4** at around 620 and 670 nm. The strongest fluorescence quenching was observed in the spectra of **Dye-1** due to the possible electron transfer from porphyrin core to the COOH group. Meanwhile, the time-resolved fluorescence spectroscopy was used to detect the fluorescence lifetime of the chlorin-type sensitizers. All profiles decay as a single exponential with a time constant τ in nanoseconds (Table 1) which is several orders of magnitude greater than that of the electron injection (in picoseconds) into the conduction band of the TiO_2 [24]. Thus, the excited electron of the four dyes could have enough time to transfer into the semiconductor under illumination.

Cyclic voltammetry was employed to determine the redox potentials of the chlorins (see Figure S5 in Supplementary Materials). All chlorin-type sensitizers show reversible oxidation waves and quasi-reversible reduction waves. The first oxidation potentials vs Fc/Fc^+ are listed in Table 2. Their first oxidation potentials corresponding to the HOMO energy of the dye are all lower than that of the I^-/I_3^- couple [71], while the LUMO energy are all higher than that of the conduction band of the TiO_2 semi-conductor. This result ensures the generation of current in the presence of sunlight. Additional one-electron oxidations are present at a potential of about 0.4 V, corresponding to the formation of the dication from the radical cation. There are also reversible one-electron reductions at around −1.4 V due to the reduction of the porphyrin ring and another irreversible one-electron reduction at about −1.8 V as a result of the reduction of the porphyrin anion.

Table 1
Absorption, fluorescence and fluorescence lifetime for porphyrins dyes.

	λ_{max}[a], nm (ε, 10^3 $M^{-1}\cdot cm^{-1}$)	Emission λ_{max}[b] (nm)	τ[c] (ns)
$\mathbf{P_0}$	420(433.3), 517(16.3), 552(8.7), 592(5.0), 648(5.3)		
Dye-1	420(240.7), 586(9.7), 614(27.7)	617, 670	1.85
Dye-2	420(240.7), 586(12.3), 613(28.7)	617, 669	1.64
Dye-3	418(243.3), 585(11.7), 612(28)	616, 671	1.72
Dye-4	418(239), 585(13), 612(29.7)	616, 670	1.69

[a] Absorption data were obtained in EtOH solution at 298 K.
[b] Emission spectra were obtained at 298 K in EtOH by exciting at 420 nm.
[c] Fluorescence lifetime was measured in argon saturated EtOH by exciting at 366 nm.

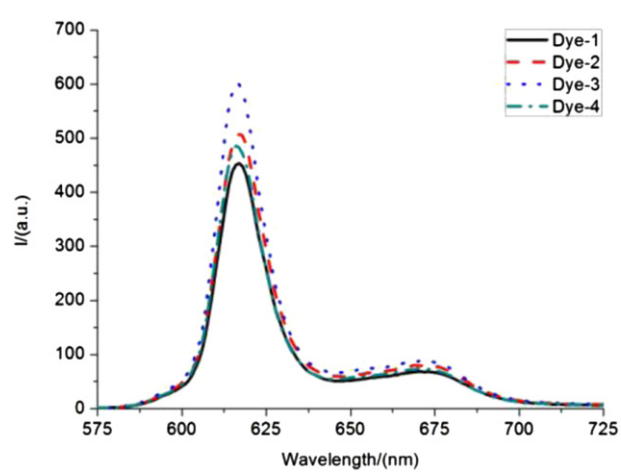

Fig. 5. The emission spectra of **Dye-1**, **Dye-2**, **Dye-3** and **Dye-4** in EtOH (3×10^{-6} mol/L, excitation at 420 nm).

Table 2
Electrochemical data for chlorin-type sensitizers.

	E_{ox}[a] (V)	HOMO[b] (eV)	E_g[c] (eV)	LUMO[d] (eV)
Dye-1	0.203	−5.003	2.01	−2.993
Dye-2	0.198	−4.998	2.00	−2.998
Dye-3	0.207	−5.007	2.01	−2.997
Dye-4	0.202	−5.002	2.01	−2.992

[a] First oxidation potentials vs ferrocene/ferrocenium (Fc/Fc^+) couple.
[b] HOMO $= -4.8$ ev $- (E_{ox1} - E_{Fc/Fc^+})$.
[c] E_g is obtained from the intersecting point between the UV–Vis spectra and the emission spectra.
[d] LUMO = HOMO + E_g.

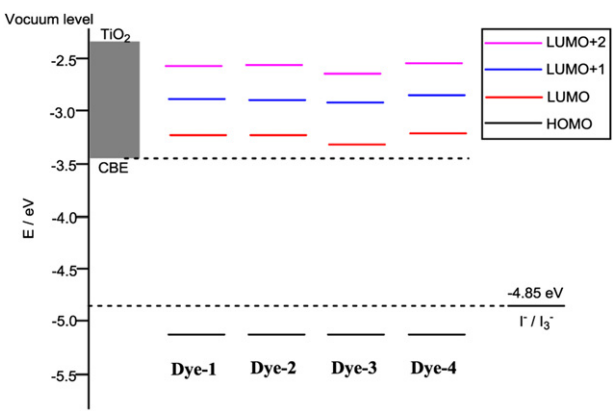

Fig. 6. Energy levels (eV) of HOMO, LUMO, LUMO + 1, and LUMO + 2 molecular orbitals for the four chlorin-type sensitizers based on DFT calculations.

3.3. DFT calculation

In order to further understand the electronic properties associated with the geometry of the four chlorin-type sensitizers with 2,6-dichlorophenyl group, *ab initio* quantum mechanical calculations were performed with the TD-DFT variant hybrid density functional theory (BP 86) in conjunction with the 6-31G(d,p) basis set as implemented in the Gaussian 09 program package [72]. The distribution of the electron cloud at the molecular orbitals HOMO, LUMO, LUMO+1 and LUMO+2 are shown in Figure S6 (in Supplementary Materials). Fig. 6 displays the molecular orbital energy levels of the four chlorin-type sensitizers which are compared with the conduction band of TiO_2 and I^-/I_3^- based on DFT calculations. The reasonable energy match between them suggests that a favourable current could be produced in these porphyrin-sensitized solar cells under sunlight.

3.4. Photovoltaic properties of porphyrin-sensitized DSSCs

Excitation of the porphyrin molecules with visible light will lead to the electronically excited state that undergoes electron-transfer quenching as a consequence of electrons being injected into the conduction band of the semiconductor. The oxidized porphyrin is subsequently reduced back to the ground state (S) by the electron donor (I^-) in the electrolyte. The electrons in the conduction band are collected and subsequently pass through the external circuit to arrive at the counter electrode. The photocurrent–photovoltage (I–V) and the incident photon-to-current conversion efficiency (IPCE) curves of the DSSCs based on the four isomeric chlorin-type sensitizers have been measured (Fig. 7 and Table 3), in which the **Zn-3** [73] (see Supplementary Materials, Figure S3) was used as reference in the DSSCs. The same photovoltaic performance order, **Dye-1**>**Dye-4**>**Dye-2**>**Dye-3**, were observed in the I–V curves and the IPCE profiles. This order is consistent with that of the Q band absorption properties of the chlorin-type sensitizers in TiO_2 films. Thus, this result demonstrates the significance of the absorption in long-wavelength on the overall solar energy conversion capability. In addition, through measuring surface coverage (Γ) of each sensitizer (**Dye-2**>**Dye-1**>**Dye-4**>**Dye-3**), we have found that the amount of dyes adsorbed onto the TiO_2 film was not proportional to the photovoltaic performance. **Dye-2** attains the maximum Γ value, however, its solar energy conversion capability in DSSCs locates in the middle among the four dyes. For **Dye-2** with the dichlorophenyl group oriented to the 10-position (opposite to COOH group), this structure is prone to aggregation which could lead to the suggested exciton annihilation [43,74] when anchored onto a TiO_2 film and consequently leads to a decrease of conversion efficiency (η) in spite of the maximum Γ. On the other hand, **Dye-3** with the dichlorophenyl group oriented towards the 20-position (COOH group) makes itself difficult to anchor onto TiO_2 film, and affords the minimum Γ value as well as the poorest photovoltaic performance. By contrast, **Dye-1** and **Dye-4** with the dichlorophenyl group oriented to the 5- or 15-position give the middle Γ value. In their condition, the dichlorophenyl group doesn't block anchorage onto TiO_2 films and can also reduce the aggregation of sensitizers. Therefore, **Dye-1** and **Dye-4** give better photovoltaic performance among the four chlorin-type sensitizers. So, the photovoltaic performance was also closely bound with the stereo-structures of the four sensitizers. In brief, we have realized that the η exhibited close relationship with the Q band absorption in TiO_2 films and the "spatial orientation" of the dichlorophenyl group. When the sensitizer has a stronger Q band absorption intensity after connecting with TiO_2 films and the steric hindrance group orients to the *meso*-substituent being perpendicular to the *meso*-position of the anchor group, it will give better performance in the DSSCs. In our study,

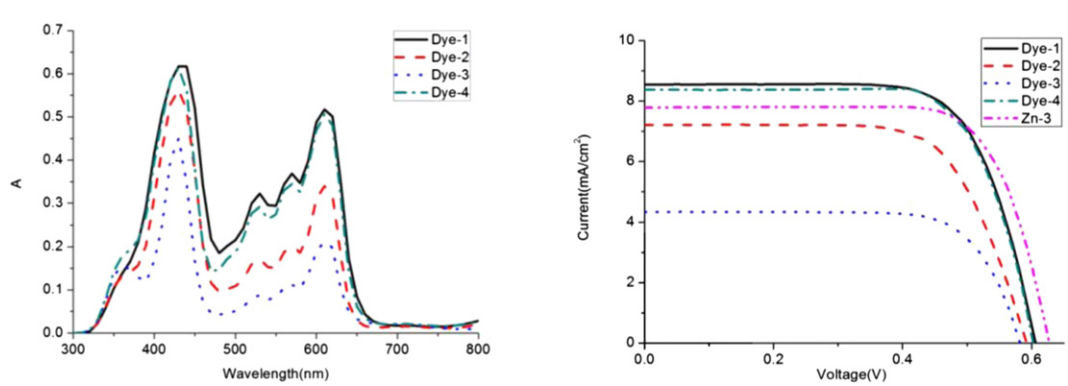

Fig. 7. The IPCE profiles (left) and the I–V curves of the chlorin-type sensitizers (right).

Table 3
The constants of the DSSCs based on the chlorin-type sensitizers.

Dyes	Γ, mol/cm^2	J_{sc}, mA/cm^2	V_{oc}, V	FF	η, %
Zn-3		7.78	630	72.94	3.57
Dye-1	8.55×10^{-8}	8.55	610	69.96	3.65
Dye-2	1.17×10^{-7}	7.21	600	67.41	2.92
Dye-3	5.39×10^{-8}	4.35	590	72.06	1.85
Dye-4	7.85×10^{-8}	8.37	600	71.38	3.60

Dye-1 gave the highest efficiency of 3.65% with a short circuit photocurrent density of 8.55 mA/cm^2, an open-circuit voltage of 610 mV, and a fill factor of 0.70 under the standard illumination test conditions.

4. Conclusions

In summary, the artificial chlorin-type sensitizers with high absorption above 600 nm have been implemented in DSSCs. We find that the photovoltaic performance of the four sensitizers closely relates with the Q band absorption after being deposited on TiO_2 film and the stereo-structures of the sensitizers. The increasing Q band absorption will improve the total conversion efficiency from solar energy to electricity. On the other hand, the steric hindrance group being perpendicular to the anchor group will give a positive effect on the capacity of converting solar energy for this kind of chlorin-type sensitizers, while the steric hindrance of the anchor group will have a negative effect. The results offer a new proposed strategy to the design of chlorin-type sensitizer for better utilization of solar energy in future. However, 4-carboxyphenyl group and the porphyrin framework are not coplanar due to the steric hindrance in space, in which the electron transfer would be blocked. Thus introduction of the alkyne or alkene or a thiophene ring [24–27] between them could be a reasonable way to enhance the electron transfer from excited porphyrin under light. In addition, inspired by Wang's work [70], addition of some coadsorbent, e.g. CDCA or other organic dyes, could be another potential method to improve the photovoltaic performance of chlorin-type sensitizers. Further work on these is in progress.

Acknowledgements

We thank Prof. Dr. Song Xue for the measurement of IPCE. This work is supported by National Natural Science Foundation of China (No. 21076147), Natural Science Foundation of Tianjin (No. 10JCZDJC23700), National International S&T Cooperation Foundation of China (No. 2012DFG41980) and Independent Innovation Foundation of Tianjin University (2010).

Appendix A. Supplementary data

Supplementary data related to this article can be found at http://dx.doi.org/10.1016/j.dyepig.2013.01.013.

References

[1] O'Regan B, Grätzel M. A low-cost, high-efficiency solar cell based on dye-sensitized colloidal TiO_2 films. Nature 1991;353:737–40.
[2] Velusamy M, Justin Thomas KR, Lin JT, Hsu YC, Ho KC. Organic dyes incorporating low-band-gap chromophores for dye-sensitized solar cells. Org Lett 2005;7(10):1899–902.
[3] Liang M, Xu W, Cai F, Chen P, Peng B, Chen J, et al. New triphenylamine-based organic dyes for efficient dye-sensitized solar cells. J Phys Chem C 2007;111(11):4465–72.
[4] Hagberg DP, Yum JH, Lee H, De Angelis F, Marinado T, Karlsson KM, et al. Molecular engineering of organic sensitizers for dye-sensitized solar cell applications. J Am Chem Soc 2008;130(19):6259–66.
[5] Cheng X, Sun S, Liang M, Shi Y, Sun Z, Xue S. Organic dyes incorporating the cyclopentadithiophene moiety for efficient dye-sensitized solar cells. Dyes Pigments 2012;92(3):1292–9.
[6] Wu W, Yang J, Hua J, Tang J, Zhang L, Lomg Y, et al. Efficient and stable dye-sensitized solar cells based on phenothiazine sensitizers with thiophene units. J Mater Chem 2012;20(9):1772–9.
[7] Ying W, Guo F, Li J, Zhang Q, Wu W, Tian H, et al. Series of new D-A-pi-A organic broadly absorbing sensitizers containing isoindigo unit for highly efficient dye-sensitized solar cells. ACS Appl Mater Interfaces 2012;4(8):4215–24.
[8] Tang J, Hua J, Wu W, Li J, Jin Z, Long Y, et al. New starburst sensitizer with carbazole antennas for efficient and stable dye-sensitized solar cells. Energy Environ Sci 2010;3(11):1736–45.
[9] Wang Z, Cui Y, Dan-oh Y, Kasada C, Shinpo A, Hara K. Thiophene-functionalized coumarin dye for efficient dye-sensitized solar cells: electron lifetime improved by coadsorption of deoxycholic acid. J Phys Chem C 2007;111(19):7224–30.
[10] Hara K, Kurashige M, Danoh Y, Kasada C, Shinpo A, Suga S, et al. Design of new coumarin dyes having thiophene moieties for highly efficient organic-dye-sensitized solar cells. New J Chem 2003;27:783–5.
[11] Seo KD, Choi IT, Park YG, Kang S, Lee JY, Kim HK. Novel D-A-π-A coumarin dyes containing low band-gap chromophores for dye-sensitised solar cells. Dyes Pigments 2012;94(3):469–74.
[12] Zhao HC, Harney JP, Huang YT, Yum JH, Nazeeruddin MK, Grätzel M, et al. Evaluation of a ruthenium oxyquinolate architecture for dye-sensitized solar cells. Inorg Chem 2011;51(1):1–3.
[13] Yu Z, Najafabadi HM, Xu Y, Nonomura K, Sun L, Kloo L. Ruthenium sensitizer with a thienylvinylbipyridyl ligand for dye-sensitized solar cells. Dalton Trans 2011;40(33):8361–6.
[14] Wu KL, Hsu HC, Chen K, Chi Y, Chung MW, Liu WH, et al. Development of thiocyanate-free, charge-neutral Ru(II) sensitizers for dye-sensitized solar cells. Chem Commun (Camb) 2010;46(28):5124–6.
[15] Sun Y, Onicha AC, Myahkostupov M, Castellano FN. Viable alternative to N719 for dye-sensitized solar cells. ACS Appl Mater Interfaces 2010;2(7):2039–45.
[16] Sauvage F, Chen D, Comte P, Huang F, Heiniger LP, Cheng YB, et al. Dye-sensitized solar cells employing a single film of mesoporous TiO_2 beads achieve power conversion efficiencies over 10%. ACS Nano 2010;4(8):4420–5.
[17] Han WS, Han JK, Kim HY, Choi MJ, Kang YS, Pac C, et al. Electronic optimization of heteroleptic Ru(II) bipyridine complexes by remote substituents: synthesis, characterization, and application to dye-sensitized solar cells. Inorg Chem 2011;50(8):3271–80.
[18] Yella A, Lee HW, Tsao HN, Yi C, Chandiran AK, Nazeeruddin MK, et al. Porphyrin-sensitized solar cells with cobalt (II/III)-based redox electrolyte exceed 12 percent efficiency. Science 2011;334(6056):629–34.
[19] Lu HP, Mai CL, Tsia CY, Hsu SJ, Hsieh CP, Chiu CL, et al. Design and characterization of highly efficient porphyrin sensitizers for green see-through dye-sensitized solar cells. Phys Chem Chem Phys 2009;11(44):10270–4.
[20] Liu Y, Lin H, Dy JT, Tamaki K, Nakazaki J, Nakayama D, et al. N-fused carbazole-zinc porphyrin-free-base porphyrin triad for efficient near-IR dye-sensitized solar cells. Chem Commun (Camb) 2011;47(13):4010–2.
[21] Lee CW, Lu HP, Lan CM, Huang YL, Liang YR, Yen WN, et al. Novel zinc porphyrin sensitizers for dye-sensitized solar cells: synthesis and spectral, electrochemical, and photovoltaic properties. Chemistry 2009;15(6):1403–12.
[22] Lee CY, Hupp JT. Dye sensitized solar cells: TiO_2 sensitization with a bodipy-porphyrin antenna system. Langmuir 2009;26(5):3760–5.
[23] Chang YC, Wang CL, Pan TY, Hong SH, Lan CM, Kuo HH, et al. A strategy to design highly efficient porphyrin sensitizers for dye-sensitized solar cells. Chem Commun (Camb) 2011;47(31):8910–2.
[24] Liu Y, Xiang N, Feng X, Shen P, Zhou W, Weng C, et al. Thiophene-linked porphyrin derivatives for dye-sensitized solar cells. Chem Commun (Camb) 2009;(18):2499–501.
[25] Zhou W, Zhao B, Shen P, Jiang S, Huang H, Deng L, et al. Multi-alkylthienyl appended porphyrins for efficient dye-sensitized solar cells. Dyes Pigments 2011;91(3):404–12.
[26] Xiang N, Huang X, Feng X, Liu Y, Zhao B, Deng L, et al. The structural modification of thiophene-linked porphyrin sensitizers for dye-sensitized solar cells. Dyes Pigments 2011;88(1):75–83.
[27] Zhou W, Cao Z, Jiang S, Huang H, Deng L, Liu Y, et al. Porphyrins modified with a low-band-gap chromophore for dye-sensitized solar cells. Org Electron 2012;13(4):560–9.
[28] Qu S, Wang B, Guo F, Li J, Wu W, Kong C, et al. New diketo-pyrrolo-pyrrole (DPP) sensitizer containing a furan moiety for efficient and stable dye-sensitized solar cells. Dyes Pigments 2012;92(3):1384–93.
[29] Wan Z, Jia C, Zhou L, Huo W, Yao X, Shi Y. Influence of different arylamine electron donors in organic sensitizers for dye-sensitized solar cells. Dyes Pigments 2012;95(1):41–6.
[30] Mao M, Wang J, Xiao Z, Dai S, Song Q. New 2,6-modified BODIPY sensitizers for dye-sensitized solar cells. Dyes Pigments 2012;94(2):224–32.
[31] Qu S, Tian H. Diketopyrrolopyrrole (DPP)-based materials for organic photovoltaics. Chem Commun (Camb) 2012;48(25):3039–51.
[32] Qu S, Qin C, Islam A, Wu Y, Zhu W, Hua J, et al. A novel D-A-pi-A organic sensitizer containing a diketopyrrolopyrrole unit with a branched alkyl chain for highly efficient and stable dye-sensitized solar cells. Chem Commun (Camb) 2012;48(55):6972–4.

[33] Li W, Wu Y, Zhang Q, Tian H, Zhu W. D-A-pi-A featured sensitizers bearing phthalimide and benzotriazole as auxiliary acceptor: effect on absorption and charge recombination dynamics in dye-sensitized solar cells. ACS Appl Mater Interfaces 2012;4(3):1822–30.
[34] Burrell AK, Officer DL, Plieger PG, Reid DC. Synthetic routes to multiporphyrin arrays. Chem Rev 2001;101(9):2751–96.
[35] Tamiaki H, Shibata R, Mizoguchi T. The 17-propionate function of (bacterio) chlorophylls: biological implication of their long esterifying chains in photosynthetic systems. Photochem Photobiol 2007;83(1):152–62.
[36] Kay A, Grätzel M. Artificial photosynthesis. 1. Photosensitization of titania solar cells with chlorophyll derivatives and related natural porphyrins. J Phys Chem 1993;97(23):6272–7.
[37] Cavaleiro JA, Smith KM. Chromatography of chlorophylls and bacteriochlorophylls. Talanta 1986;33(12):963–71.
[38] Amao Y, Komori T. Bio-photovoltaic conversion device using chlorine-e6 derived from chlorophyll from Spirulina adsorbed on a nanocrystalline TiO_2 film electrode. Biosens Bioelectron 2004;19(8):843–7.
[39] Koyama Y, Miki T, Wang X, Nagae H. Dye-sensitized solar cells based on the principles and materials of photosynthesis: mechanisms of suppression and enhancement of photocurrent and conversion efficiency. Int J Mol Sci 2009; 10(11):4575–622.
[40] Wang X, Koyama Y, Wada Y, Sasaki S-i, Tamiaki H. A dye-sensitized solar cell using pheophytin–carotenoid adduct: enhancement of photocurrent by electron and singlet-energy transfer and by suppression of singlet–triplet annihilation due to the presence of the carotenoid moiety. Chem Phys Lett 2007;439(1–3):115–20.
[41] Wang X, Tamiaki H. Cyclic tetrapyrrole based molecules for dye-sensitized solar cells. Energy Environ Sci 2010;3:94–106.
[42] Wang X, Koyama Y, Kitao O, Wada Y, Sasaki SI, Tamiaki H, et al. Significant enhancement in the power-conversion efficiency of chlorophyll co-sensitized solar cells by mimicking the principles of natural photosynthetic light-harvesting complexes. Biosens Bioelectron 2010;25(8):1970–6.
[43] Wang X, Tamiaki H, Wang L, Tamai N, Kitao O, Zhou H, et al. Chlorophyll-a derivatives with various hydrocarbon ester groups for efficient dye-sensitized solar cells: static and ultrafast evaluations on electron injection and charge collection processes. Langmuir 2010;26(9):6320–7.
[44] Tomé AC, Lacerda PSS, Neves MGPMS, Cavaleiro JA. meso-Arylporphyrins as dienophiles in Diels–Alder reactions: a novel approach to the synthesis of chlorins, bacteriochlorins and naphthoporphyrins. Chem Commun 1997: 1199–200.
[45] Whitlock HW, Hanauer R, Oester MY, Bower BK. Diimide reduction of porphyrins. J Am Chem Soc 1969;91(26):7485–9.
[46] Kozyrev AN, Dougherty TJ, Pandey RK. Effect of substituents in OsO_4 reactions of metallochlorins regioselective synthesis of isobacteriochlorins and bacteriochlorins. Tetra Lett 1996;37(22):3781–4.
[47] Li X, Zhuang J, Li Y, Liu H, Wang S, Zhu D. Synthesis of isoxazoline-fused chlorins and bacteriochlorins by 1,3-dipolar cycloaddition reaction of porphyrin with nitrile oxide. Tetra Lett 2005;46(9):1555–9.
[48] Liu X, Feng Y, Hu X, Li X. Synthesis of novel isoxazole-fused chlorins and bacteriochlorins via 1,3-dipolar cycloaddition reactions of nitrile oxides with porphyrins. Synthesis 2005;(20):3632–8.
[49] Silva AM, Lacerda PS, Tomé AC, Neves MG, Cavaleiro JA, Makarova EA, et al. Porphyrins in 1,3-dipolar cycloaddition reactions. Synthesis of new porphyrin-chlorin and porphyrin-tetraazachlorin dyads. J Org Chem 2006; 71(22):8352–6.
[50] Silva AM, Tomé AC, Neves MG, Cavaleiro JA. 1,3-Dipolar cycloaddition reactions of porphyrins with azomethine ylides. J Org Chem 2005;70(6):2306–14.
[51] Lopez-Perez A, Robles-Machin R, Adrio J, Carretero JC. Oligopyrrole synthesis by 1,3-dipolar cycloaddition of azomethine ylides with bissulfonyl ethylenes. Angew Chem Int Ed Engl 2007;46(48):9261–4.
[52] Silva AMG, Tomé AC, Neves MGPMS, Silva AMS, Cavaleiro JA, Perrone D, et al. Porphyrins in 1,3-dipolar cycloaddition reactions with sugar nitrones. Synthesis of glycoconjugated isoxazolidine-fused chlorins and bacteriochlorins. Tetra Lett 2002;43(4):603–5.
[53] Wang GW, Yang HT, Wu P, Miao CB, Xu Y. Novel cycloaddition reaction of [60] fullerene with carbonyl ylides generated from epoxides. J Org Chem 2006; 71(11):4346–8.
[54] Barkawi LS, Cohen JD. A method for concurrent diazomethane synthesis and substrate methylation in a 96-sample format. Nat Protoc 2010;5(10):1619–26.
[55] Adler AD, Longo FR, Finarelli JD, Goldmacher J, Assour J, Korsakoff L. A simplified synthesis for meso-tetraphenylporphine. J Org Chem 1967;32(2): 476–476.
[56] Yanagida M, Yamaguchi T, Kurashige M, Fujihashi G, Hara K, Katoh R, et al. Nanocrystalline solar cells sensitized with monocarboxyl or dicarboxyl pyridylquinoline ruthenium(II) complexes. Inorg Chim Acta 2003;351:283–90.
[57] Ito S, Murakami TN, Comte P, Liska P, Grätzel C, Nazeeruddin MK, et al. Fabrication of thin film dye sensitized solar cells with solar to electric power conversion efficiency over 10%. Thin Solid Films 2008;516(14):4613–9.
[58] Yan S, Bu Y, Cao Z, Li P. Coupling character between imidazole and imidazole cation: implication for the coupling modes of biomolecular residues. J Phys Chem A 2004;108:7038–49.
[59] Wan L, Qi D, Zhang Y, Jiang J. Controlling the directionality of charge transfer in phthalocyaninato zinc sensitizer for a dye-sensitized solar cell: density functional theory studies. Phys Chem Chem Phys 2011;13(4):1639–48.
[60] Wan L, Qi D, Zhang Y. The effect of beta-saturated pyrrolic rings on the electronic structures and aromaticity of magnesium porphyrin derivatives: a density functional study. J Mol Graph Model 2011;30:15–23.
[61] Qi D, Zhang Y, Zhang L, Jiang J. Structures and spectroscopic properties of fluoroboron–subtriazaporphyrin derivatives: density functional theory approach on the benzo-fusing effect. J Phys Chem A 2010;114:1931–8.
[62] Qi D, Zhang L, Wan L, Zhang Y, Bian Y, Jiang J. Conformational effects, molecular orbitals, and reaction activities of bis(phthalocyaninato) lanthanum double-deckers: density functional theory calculations. Phys Chem Chem Phys 2011;13(29):13277–86.
[63] Zhang L, Qi D, Zhang Y, Bian Y, Jiang J. Density functional theory studies on the structures and electronic communication of meso-ferrocenylporphyrins: long range orbital coupling via porphyrin core. J Mol Graph Model 2011;29(5): 717–25.
[64] Qi D, Zhang L, Zhang Y, Bian Y, Jiang J. Nature of the intense near-IR absorption and unusual broad UV–Visible-NIR spectra of azulenocyanines: density functional theory studies. J Phys Chem A 2010;114(51):13411–7.
[65] Peralta GA, Seth M, Zhekova H, Ziegler T. Magnetic circular dichroism of phthalocyanine (m = mg, zn) and tetraazaporphyrin (m = mg, zn, ni) metal complexes. A computational study based on time-dependent density functional theory. Inorg Chem 2008;47(10):4185–98.
[66] Nemykin VN, Hadt RG, Belosludov RV, Mizuseki H, Kawazoe Y. Influence of molecular geometry, exchange-correlation functional, and solvent effects in the modeling of vertical excitation energies in phthalocyanines using time-dependent density functional theory (TDDFT) and polarized continuum model TDDFT methods: can modern computational chemistry methods explain experimental controversies. J Phys Chem A 2007;111(50):12901–13.
[67] Lee SU, Kim JC, Mizuseki H, Kawazoe Y. The origin of the halogen effect on the phthalocyanine green pigments. Chem Asian J 2010;5:1341–6.
[68] Donzello MP, Ercolani C, Kadish KM, Ricciardi G, Rosa A, Stuzhin PA. Tetrakis(thiadiazole)porphyrazines. 5. Electrochemical and DFT/TDDFT studies of the free-base macrocycle and its MgII, ZnII, and CuII complexes. Inorg Chem 2007;46(10):4145–57.
[69] Zhou J, Liu J, Feng Y, Wei S, Gu X, Wang X, et al. Synthesis and characterization of the monomer ruthenium complex of hypocrellin B. Bioorg Med Chem Lett 2005;15(12):3067–70.
[70] Wang X, Kitao O, Zhou H, Tamiaki H, Sasaki S-i. Efficient dye-sensitized solar cell based on oxo-bacteriochlorin sensitizers with broadband absorption capability. J Phys Chem C 2009;113(18):7954–61.
[71] Balanay MP, Kim DH. DFT/TD-DFT molecular design of porphyrin analogues for use in dye-sensitized solar cells. Phys Chem Chem Phys 2008;10(33): 5121–7.
[72] Frisch MJ, Trucks GW, Schlegel HB, Scuseria GE, Robb MA, Cheeseman JR, et al. Gaussian 09 (Revision A.2). Wallingford, CT: Gaussian, Inc.; 2009.
[73] Wang Q, Campbell WM, Bonfantani EE, Jolley KW, Officer DL, Walsh PJ, et al. Efficient light harvesting by using green Zn-porphyrin-sensitized nanocrystalline TiO_2 films. J Phys Chem B 2005;109(32):15397–409.
[74] Campbell WM, Jolley KW, Wagner P, Wagner K, Walsh PJ, Gordon KC, et al. Highly efficient porphyrin sensitizers for dye-sensitized solar cells. J Phys Chem C 2007;111(32):11760–2.